*BJR*, 2026, **99**, 206–217
https://doi.org/10.1093/bjr/tqaf297
Advance access publication: 3 December 2025
**Review**

# Staging pleural mesothelioma revitalized

**Rachel E Benamore, MA, MB BChir[1,*], Cheng Xie, DPhil, PGDip, MBChB[1]**
**Ikboljon Sobirov, MSc[*,2]**

[1]Department of Radiology, Oxford University Hospitals NHS Foundation Trust, Oxford OX3 7LJ, United Kingdom
[2]Acute Multidisciplinary Imaging and Interventional Centre, Division of Cardiovascular Medicine, Radcliffe Department of Medicine, University of Oxford, Oxford OX3 9DU, United Kingdom

*Corresponding authors: Ikboljon Sobirov, MSc, Acute Multidisciplinary Imaging and Interventional Centre, Division of Cardiovascular Medicine, Radcliffe Department of Medicine, University of Oxford, John Radcliffe Hospital, Headington OX3 9DS, United Kingdom (ikboljon.sobirov@cardiov.ox.ac.uk) and Rachel E. Benamore, MA, MB BChir, Department of Radiology, Surgery and Diagnostics Building, Churchill Hospital, Oxford University Hospitals NHS Foundation Trust, Old Road, Headington, Oxford OX3 7LJ, United Kingdom (rachel.benamore@ouh.nhs.uk)

## Abstract

Malignant pleural mesothelioma (PM) is the most common primary tumour of the pleura. Accurate staging is essential for treatment selection and prognostication. The 9th edition of the TNM classification introduces validated, imaging-based updates to tumour (T), node (N), and metastasis (M) staging. This article explores the scientific rationale and clinical utility of TNM 9, with a focus on imaging techniques, automated tumour volume assessment, and future developments in imaging and artificial intelligence.

## Introduction

Pleural mesothelioma (PM) is the most common primary tumour of the pleura. Although PM cases in the UK appear to be starting to fall, it still represents a significant disease burden, with over 2200 deaths per year.[1] Given that most patients are not surgical candidates, imaging plays a vital role in staging and guiding treatment. This review explores recent revisions to the staging system, particularly the 9th edition of the TNM classification (TNM 9),[2] and discusses the roles of CT, MRI, PET, and artificial intelligence in accurate disease evaluation.

## Staging of pleural mesothelioma with imaging

Staging PM is challenging due to its diffuse, rind-like growth. Traditional size-based criteria are ineffective. Assessment of T stage was adapted from surgical staging and was based on local tumour invasion, rather than tumour size, as often tumour is resected piece meal at surgery. This is prone to intra- and interobserver variation, with variable prognostic accuracy.[3-5] PM thickness measurements were first collected systematically in the database used to develop the 8th edition of the TNM classification system (TNM 8)[6,7] and suggested prognostic significance. TNM 9[2] builds on this by refining imaging-based measurements and validating them across large international cohorts. Although still biased towards patients undergoing surgery with palliative and curative intent (31.9% and 36.4%, respectively), the TNM 9 database contains the largest proportion of patients treated non-surgically, with a better geographical distribution.

### Primary tumour (T) classification

Tumour volume has been found to predict survival and time to recurrence in both surgical and non-surgical patients,[5,7-11] confirming the need for a size descriptor for the T category (Table 1). However, there is neither standardization nor the ability of many institutions to measure PM volume on imaging. A simple approach that has potential for widespread adoption is needed. Unidimensional pleural thickness measurements were initially explored during the 8th edition revision[12] and found to be promising. They are also established parameters in the Revised Modified Response Evaluation Criteria in Solid Tumours for Assessment of Response in Malignant Pleural Mesothelioma (Version 1.1).[13]

Gill et al[14] analysed worldwide data based on 3598 patients (2013-2022) with pathologically proven PM. Only data from CT measurements were analysed, as it is the modality most frequently used to assess the pleura and is widely available. The thorax was divided into 3 portions craniocaudally: lung apex to top of aortic arch (upper), top of aortic arch to the top of left atrium (middle), and below the top of the left atrium (lower). Maximum pleural thickness measurements at the upper (p1max), middle (p2max), and lower (p3max) hemithorax were then added together to create a Psum measurement. Fissural thickness (Fmax) was also measured perpendicular to the fissures and measurements of maximum diaphragmatic pleural thickness (Dmax) were also recorded.

A total of 1965 patients were evaluated for clinical staging and 457 for pathological staging of pleural mesothelioma, predominantly from Asia, Europe, and North America. CT-derived pleural thickness (Psum) was available in 1790 patients, averaging 45.5 mm. Diaphragmatic thickness (Dmax) and fissural thickness (Fmax) were measured in 889 and 877 patients, respectively, with averages of 11.3 and 9.6 mm. Analysis of clinical T (cT) data showed that both Psum and anatomical tumour involvement were critical in defining T categories that correlate with overall survival (OS).

**Received:** 29 June 2025; **Revised:** 11 October 2025; **Accepted:** 14 November 2025

**Table 1.** 9th edition T classification.

| Category | Clinical T (cT) | Pathological T (pT) |
|---|---|---|
| Tx | Tumour cannot be assessed | Tumour cannot be assessed |
| T0 | No tumour is present | No tumour is present |
| T1 | Tumour limited to the ipsilateral pleura with Psum ≤12 mm with no involvement of the fissure (Fmax ≤5 mm) | Tumour limited to the ipsilateral pleura with no involvement of the fissure |
| T2 | Tumour involving the ipsilateral pleura with Psum ≤12 mm and with any of the following:<br>• Involvement of the fissure (Fmax >5 mm)<br>• Mediastinal fat invasion<br>• Solitary area of chest wall soft tissue invasion<br>Or:<br>Tumour involving the ipsilateral pleura with Psum >12 mm but ≤30 mm, with or without:<br>• Involvement of the fissure (Fmax >5 mm)<br>• Mediastinal fat invasion<br>• Solitary area of chest wall soft tissue invasion | Tumour involving the ipsilateral pleura and with any of the following:<br>• Involvement of the fissure<br>• Ipsilateral lung parenchyma invasion<br>• Diaphragm (non-transmural) invasion |
| T3 | Tumour involving the ipsilateral pleura with Psum >30 mm, with or without:<br>• Involvement of the fissure (Fmax > 5mm)<br>• Mediastinal fat invasion<br>• Solitary area of chest wall soft tissue invasion | Tumour limited to the ipsilateral pleura (with or without fissure involvement) and with invasion of any of the following:<br>• Mediastinal fat<br>• Surface of pericardium<br>• Endothoracic fascia<br>• Solitary area of chest wall soft tissue |
| T4 | Tumour with invasion of any of the following (any Psum):<br>• Chest wall bony invasion (rib)<br>• Mediastinal organs (heart, spine, oesophagus, trachea, great vessels)<br>• Diffuse chest wall invasion<br>• Direct tumour extension through the diaphragm or pericardium<br>• Direct extension to the contralateral pleura<br>• Presence of malignant pericardial effusion | Tumour with invasion of any of the following:<br>• Chest wall bony invasion (rib)<br>• Mediastinal organs (heart, spine oesophagus, trachea, great vessels)<br>• Diffuse chest wall invasion<br>• Transmural invasion of the diaphragm or pericardium<br>• Direct extension to the contralateral pleura<br>• Presence of malignant pericardial effusion |

Psum = pmax1 + pmax2 + pmax3 (sum of 3 measurements of maximal pleural thickness measured on axial images along the chest wall or mediastinum in each of the 3 divisions of the chest—upper, middle, and lower divided by 2 lines; 1 at the top of the aortic arch and the second drawn at the top of the left atrium). It has not been specified whether measurements should be rounded before adding together to calculate the Psum. Fmax = maximal thickness of pleural tumour along the fissures measured on sagittal images.

Patients classified as T1 but with Fmax >5 mm had OS similar to 8th edition T2 cases, highlighting fissural involvement as an independent adverse prognostic marker.

The TNM 8 descriptors of non-transmural diaphragmatic invasion (cT2), lung parenchymal invasion (cT2), and endothoracic fascia invasion (cT3), were found unreliable on CT[7] and were removed. This led to no distinction under previous criteria between T1, T2, and T3 tumours (staged solely by endothoracic fascia invasion). However, TNM 8 T4 descriptors (deep pericardial or trans-diaphragmatic invasion, mediastinal or diffuse chest wall invasion) were strongly associated with poor prognosis irrespective of Psum and were retained in TNM 9.

TNM 9 defines T1 as Psum <12 mm, T2 as >12 and <30 mm, and T3 as ≥31 mm, with median OS of 49.8, 27.5, and 21.1 months, respectively. T4 tumours had a median OS of 12.6 months. TNM 9's cT classification demonstrated improved prognostic stratification over TNM 8. Due to limitations in pathological orientation of surgical specimens, most qualitative pathological T (pT) descriptors were retained from TNM 8, except fissural involvement, now reclassified as T2 (Table 1). Figures 1-4 show examples of the different T stages.

## N (nodal) classification

The lymphatic drainage of the visceral pleura mirrors that of the lung but parietal pleural lymphatic drainage is different and can be thought of as an envelope of nodes surrounding the pleura (Table 2).[15] There is free communication of lymphatics above and below the diaphragm and, as PM commonly involves the diaphragmatic pleural surface, a thorough search for peridiaphragmatic, posterior mediastinal, retrocrural and gastrohepatic nodes should also be undertaken. Billé et al[16] evaluated lymph node classifications in PM based on data from an international cohort of 2836 patients and found no significant survival difference between patients with single versus multiple N1 nodal stations or between those with varying numbers of involved nodes, leading to the decision to retain a simplified N classification in TNM 9. The authors recommend maintaining the current categories (N1 and N2) without further sub-classification, as this structure remains clinically relevant and supported by outcome data (Figure 5).

## Distant metastases (M) classification

In the TNM 9 revision, data from 3221 pleural mesothelioma patients, including 228 with metastatic disease at diagnosis, represent the largest cohort with detailed metastasis documentation.[17] Patients with metastases had significantly poorer median OS (10.5 vs. 21.5 months) and lower 1-year survival rates (46% vs. 71%) compared to non-metastatic patients. Among 158 cases with detailed organ involvement, no significant survival differences were found between single versus multiple organ metastases or between intrathoracic

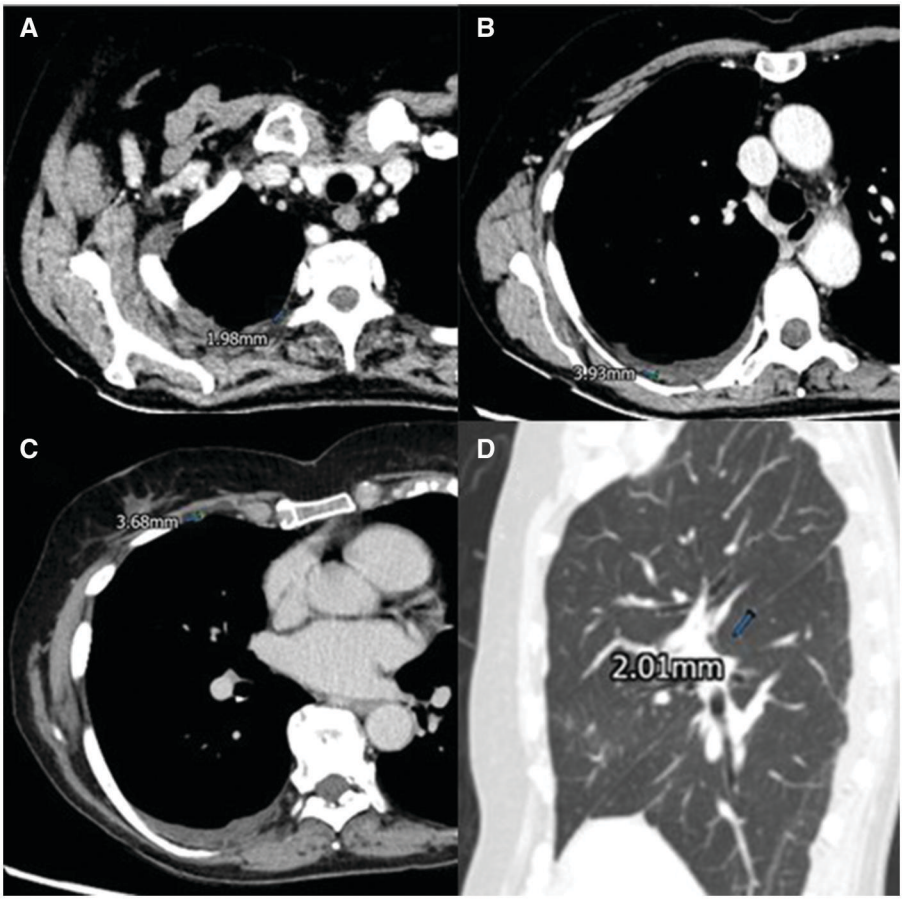


**Figure 1.** T1 tumour. A-D. T1 epithelioid mesothelioma, diagnosed via thoracoscopy. There is a small right pleural effusion, with minimal, subtly irregular pleural thickening extending onto the mediastinal surface. The images show P1max measurement in the upper zone (A), P2 max measurement in the mid zone (B), P3 max measurement in the right lower zone (C) and an Fmax measurement of <5 mm, with the subtle fissural nodularity only visible on lung windows (D), with a Psum measurement <12 mm. P measurements are obtained by measuring the maximal pleural thickness in each zone, perpendicular to the curvature of the pleural surface.

and distant metastatic sites. Due to the lack of prognostic distinction, the M classification remains binary: M0 for no metastases and M1 for metastatic disease.

### Stage groups

Nowak et al[18] analysed data from 2192 patients for clinical staging and 445 for pathological staging to propose updated stage groupings TNM 9. The study recommends combining stages IA and IB into a single stage I and reclassifying T2N0M0 as stage II to better reflect survival differences. All T3 (N0-2) M0 tumours are now classified as stage IIIA. All T4 (N0-2) M0 tumours are still classified as stage IIIB. Although the difference in OS between clinical stages IIIB and IV did not meet statistical significance, a decision was made to limit clinical stage IV to patients presenting with M1 disease, thereby maintaining the convention for cTNM classification (Table 3).

### Determining resectability

The role of surgery in treating PM remains uncertain. The MesoVATS trial[19] found that VATS partial pleurectomy (VATS-PP) offered no survival benefit compared to talc pleurodesis, which was preferred due to fewer complications and shorter hospital stays. The MARS 2 trial[20] compared extended pleurectomy-decortication plus chemotherapy with chemotherapy alone, showing longer survival and better quality of life in the non-surgical group. However, its inclusion of poor prognosis patients limits broad applicability, though its findings have led to reduced radical surgery use. Multifocal chest wall invasion, involvement of critical mediastinal structures, contralateral nodal or pleural metastases, lung or extra-thoracic metastases, and, in some cases, full-thickness diaphragmatic invasion are contraindications to pleurectomy. Radiologists must understand resectability criteria and the strengths and weaknesses of imaging modalities. American and European guidelines emphasize a multidisciplinary approach to preoperative planning, with European recommendations highlighting MRI alongside CT for improved assessment.[21,22]

## Optimizing the accuracy of staging with imaging

### Current utility of CT

CT is the primary modality for PM diagnosis, staging, and therapy response assessment in routine practice and clinical trials worldwide. However, it has limited contrast resolution and may struggle to differentiate malignant pleural disease from complex fluid or adjacent normal tissues such as atelectatic lung, diaphragm, or chest wall musculature.[23] This has

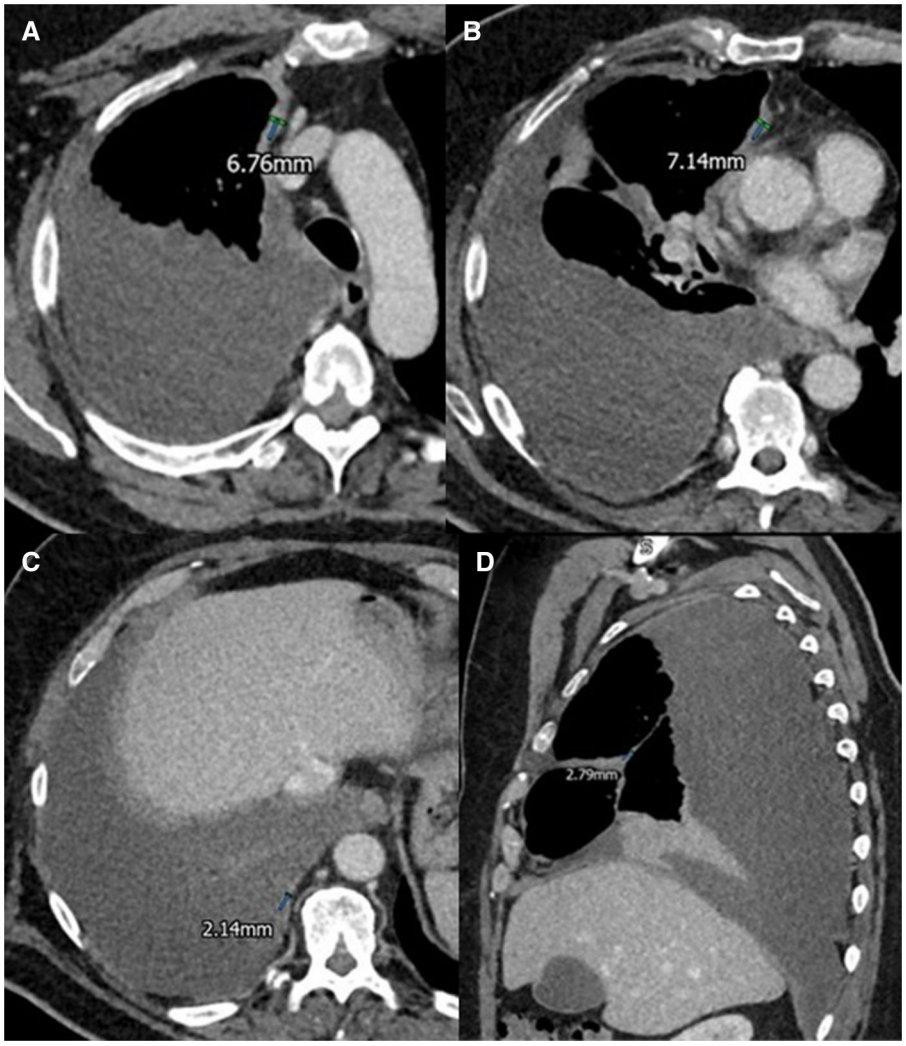


**Figure 2.** T2 tumour. A-D. T2 epithelioid mesothelioma, diagnosed via thoracoscopy. There is a large right pleural effusion, with irregular circumferential pleural thickening. The images show P1max measurement in the upper zone (A), P2 max measurement in the mid zone (B), P3 max measurement in the right lower zone (C) with a Psum measurement between 13 and 30 mm. The Fmax measurement is <5 mm.

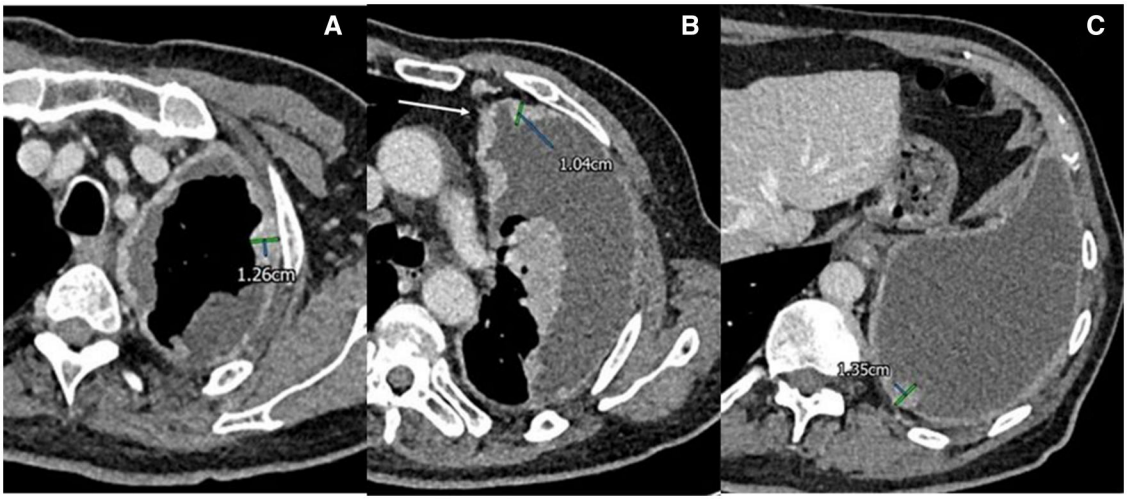


**Figure 3.** T3 tumour. A-C. T2 epithelioid mesothelioma, diagnosed via ultrasound guided pleural biopsy. There is a large left pleural effusion, with irregular circumferential pleural thickening. The images show P1max measurement in the upper zone (A), P2 max measurement in the mid zone (B), P3 max measurement in the right lower zone (C) with a Psum measurement >30 mm. Fissural tumour cannot be assessed due to the significant lung collapse. B, Invasion into the mediastinal fat (white arrow), another T3 descriptor.

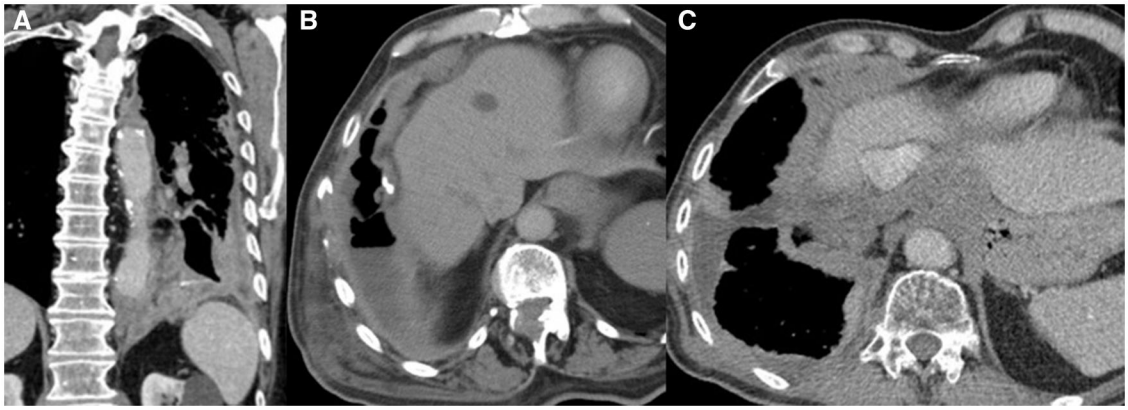


**Figure 4.** T4 tumour. A-C. Examples of T4 mesothelioma. There is transdiaphragmatic tumour spread, with tumour distorting the contour of the left hemidiaphragm and obliterating the fat between diaphragm and spleen, which is often better appreciated on sagittal or coronal reformats (A). A right sided mesothelioma is invading the lateral 6th and 7th ribs (B). A right-sided mesothelioma is infiltrating the right diaphragmatic crus (which is nodular in contour), encircles the oesphagus and extends into the left hemithorax to involve the left diaphragmatic crus (C).

**Table 2.** 9th edition N classification.

| Category | Clinical N (cN) and pathological N (pN) descriptors |
|---|---|
| Nx | Regional lymph nodes cannot be assessed |
| N0 | No regional lymph node metastasis |
| N1 | Metastases to ipsilateral intrathoracic lymph nodes (includes ipsilateral bronchopulmonary, hilar, subcarinal, paratracheal, aortopulmonary, para-esophageal, peri-diaphragmatic, pericardial fat pad, intercostal, and internal mammary nodes) |
| N2 | Metastases to contralateral lymph nodes. Metastases to ipsilateral or contralateral supraclavicular lymph nodes |

**Table 3.** Stage groups.

| | N0 | N1 | N2 |
|---|---|---|---|
| T1 | I | II | IIIA |
| T2 | II | IIIA | IIIA |
| T3 | IIIA | IIIA | IIIA |
| T4 | IIIB | IIIB | IIIB |
| M1 | IV | IV | IV |

**Figure 5.** Nodal disease. T4 N2 M1 left mesothelioma. There is diffuse posterior chest wall invasion, with associated rib destruction. There are enlarged ipsi- and contralateral mediastinal nodes, ipsilateral internal mammary nodes and contralateral posterior intercostal nodes. Although axillary nodes are anatomically adjacent to the pleural space and involved in the drainage of the chest wall, they are not currently considered part of the nodal staging in TNM 9 for mesothelioma and should be viewed as M1 disease.

contributed to perception errors and poor inter-observer variation.[4,24] Detection of early-stage PM with CT can also be challenging because macroscopic pleural nodules are frequently absent and pleural effusion may be the only visible feature, thus the low sensitivity (60%-65%) of contrast-enhanced CT in this setting.[25,26]

Accurately identifying transdiaphragmatic, transpericardial and chest wall invasion is challenging on CT, even with the use of multi-planar reformats.[27] CT often underestimates pathological stage.[4,7] When comparing surgical staging with CT staging (according to the International Union Against Cancer 7th edition of the TNM classification of malignant tumours), Rusch et al[3] showed that up to 80% of MPM patients with stage I and II disease and 23% of patients with stage III disease were upstaged at surgery.

## Current utility of MRI

PM is typically intermediate in signal intensity relative to musculature on T1- and T2-weighted imaging and avidly enhances, allowing distinction from the chest wall, diaphragm and pericardium, which are usually uniformly low in signal intensity on T1- and T2-weighted images. The primary value of MRI is to establish whether there is diaphragm, chest wall, or mediastinal invasion, in patients who are potential surgical candidates. MRI has a high sensitivity and specificity and sensitivity for detection of transdiaphragmatic spread,[28] allowing differentiation between T3 (potentially resectable) and T4 (unresectable) disease.[29] Mediastinal invasion, including pericardial invasion, can be confirmed as foci of tumour tethering on cine imaging. Other indications for MRI include characterization of equivocal adrenal lesions and of potential neural foraminal, epidural, or brachial plexus involvement.

MRI is susceptible to artefacts from respiratory or cardiac motion and susceptibility artefact from air interfaces in the

lung. Imaging obtained on both 1.5 T and 3 T magnets provide diagnostic-quality images. Diffusion-weighted imaging (DWI), measures molecular diffusion in biological tissues and is affected by tissue architecture and has been found to be promising in identification of local tumour invasion, the latter of which may be aided by using high b-value images[30] (pleural pointillism).

## Optimum timing post contrast

The pleura enhances more avidly in the venous rather than arterial phases[31] (Figure 6). However, PM is often still poorly visualized in the venous phase, which may be due to admixed pleural fibrosis.[32] In a small prospective observational study of 15 treatment-naive patients with pathologically proven PM at least 10 mm in thickness, Patel et al[33] showed maximal enhancement at a time delay of 230-300 s from contrast injection to scan acquisition, with maximal differential enhancement of tumour and muscle at approximately 240-260 seconds. Radiologists subjectively preferred a 240 seconds delay for optimal tumour visualization. Optimizing tumour enhancement may improve staging with CT and also lead to better performance of semi-automated and automated segmentation tools that are in use and under development (Figure 7).

Similar tumour enhancement kinetics have been demonstrated with contrast-enhanced MRI.[34-36] Contrast-enhanced MRI with fat suppression has been shown to be superior to CT in the identification of chest wall, transdiaphragmatic, endothoracic fascial and bone invasion,[28,29,37,38] with higher

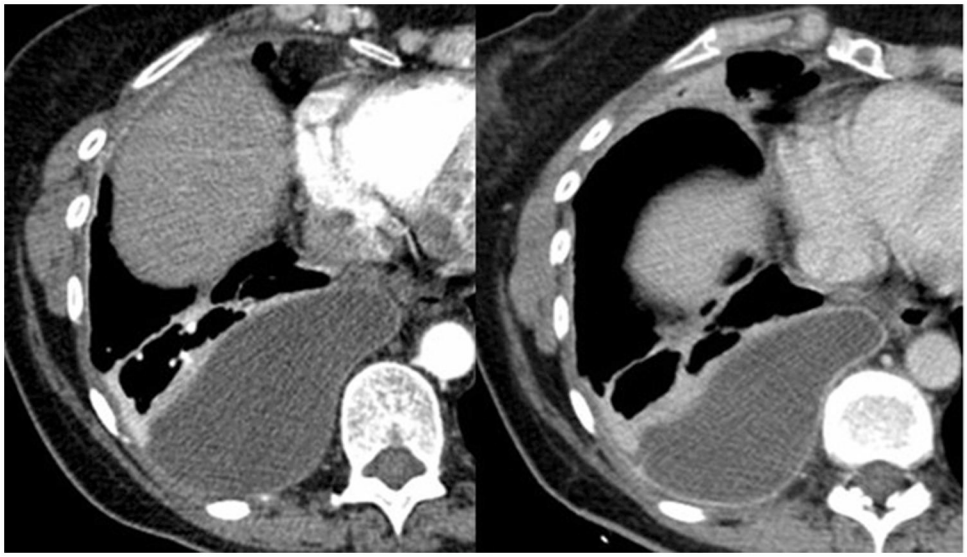

**Figure 6.** Arterial (left) and venous (right) phase images. The pleural enhancement is much more easily appreciated in the venous phase.

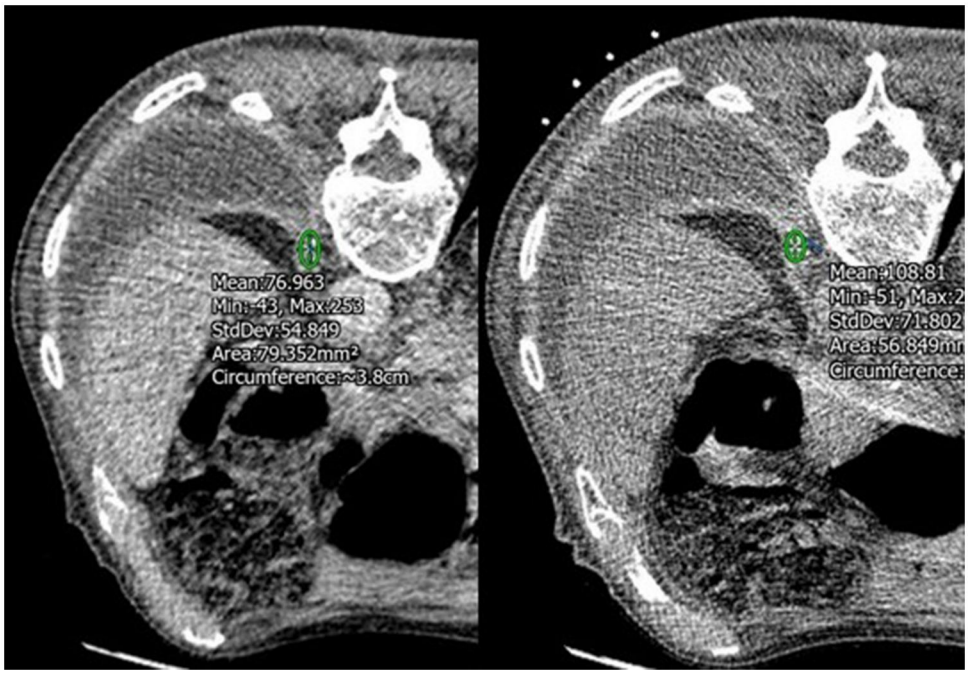


**Figure 7.** Left-sided mesothelioma, diagnosed via CT-guided pleural biopsy. The planning CT (left) was obtained in the venous phase. The right hand image shows the first image as part of the biopsy, at approximately 5 minutes after contrast. The pleural has continued to enhance.

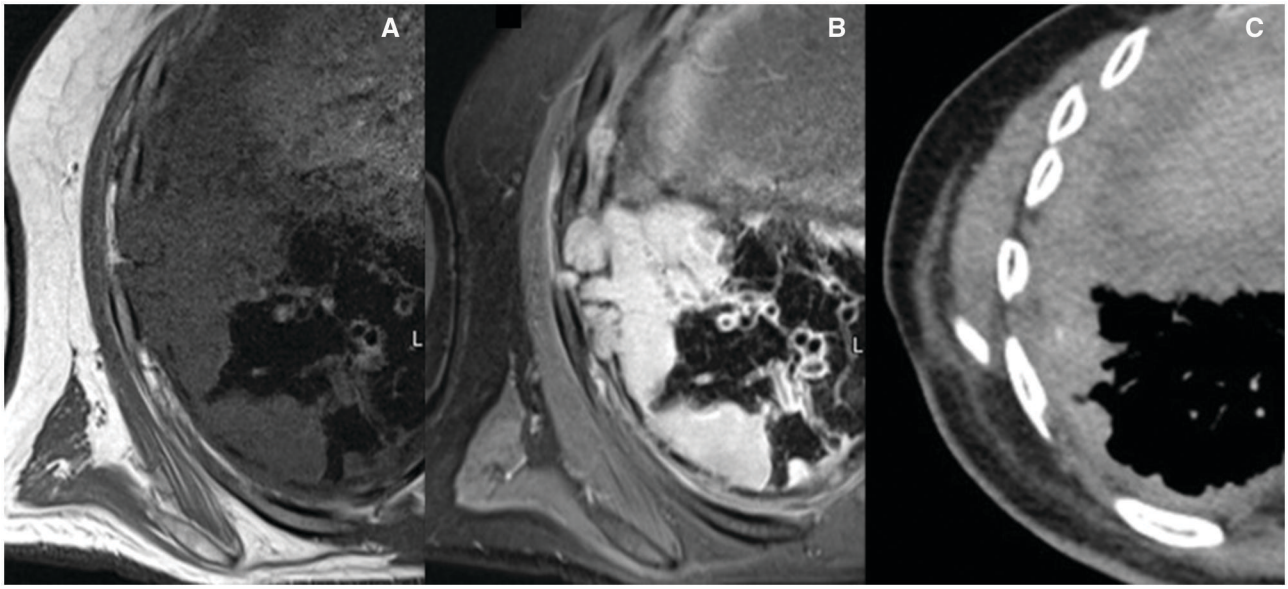


**Figure 8.** A-C. T1W axial (A), T1 fat saturated axial post-gadolinium (B) and contrast enhanced axial CT (C) images in a patient with a right sided mesothelioma. The chest wall invasion is better appreciated on the MR images and only seen as subtle loss of fat planes on contrast-enhanced CT.

inter-observer agreement[36,39] resulting in less understaging (Figure 8). Perfusion MRI and detection of early contrast enhancement has shown superior performance to contrast-enhanced CT (sensitivity 92% vs. 56% for CT) in 58 patients (84% of whom had pleural thickening <10 mm), a known limitation of CT.[40] However, clinical deployment is not feasible due to time-consuming manual post-processing requirements.

### Current utility of PET-CT

The 2-deoxy-2-[18F]fluoro-D-glucose (FDG) PET-CT contributes little to local T staging above contrast enhanced CT.[41] The main strength of FDG PET-CT in PM clinical staging is in its ability to detect occult metastases in up to 24% of patients,[42-46] and this forms an evidence-based indication for PET-CT in the UK.[47] Although metabolic behaviour of PM does not feature in current TNM staging, metabolic activity and metabolic tumour volume may have prognostic implications.[48,49]

Talc pleurodesis incites an FDG-avid inflammatory reaction in the pleura that can persist indefinitely. Although talc pleurodesis does not preclude FDG-PET-CT imaging of patients with PM, the resulting increased FDG avidity can be indistinguishable from tumour, potentially confounding tumour assessment.[49,50] Radiotherapy to the pleura, chest wall, or bone incites inflammation and subsequent intense FDG avidity, which can be a confounder in image interpretation and assessment of therapy response.

### Current recommendations for imaging pleural mesothelioma

The International Mesothelioma Interest Group (IMIG) issued recommendations in 2023 for imaging PM.[51] For CT, the panel advised scanning the chest and upper abdomen to ensure adequate coverage of the pleural space, diaphragm, and lymph nodes. A portal venous phase acquisition was recommended, with an optional delayed phase at 2-4 minutes, although optimal timing is yet to be determined. Images should be reconstructed in 3 orthogonal planes with 1-2 mm slice thickness axially and 1-3 mm coronally/sagittally, using both soft tissue and sharp kernels to assess lung and bone invasion. The entire chest wall soft tissues must be included in the field of view.

For MRI, large body coils should be positioned to encompass the diaphragm and posterior costophrenic recess, down to L3 and the full chest wall. Phase encoding should be anterior to posterior to reduce artefacts near the chest wall and diaphragm. Parallel imaging can be useful for patients with breathlessness or when assessing the pericardium. Essential sequences include 3-plane localizer, axial T1, axial/coronal T2, gradient echo, and fat-suppressed pre- and post-contrast images in 3 orthogonal planes. Dynamic post-contrast axial, sagittal, and coronal imaging is strongly recommended to assess diaphragmatic invasion, with slice thickness generally 4-6 mm. Imaging post-contrast should be acquired at 2-5 minutes, then every 1-2 minutes, depending on the contrast agent. Additional free-breathing coronal T2-weighted images, coronal short tau inversion recovery, and diffusion-weighted imaging (DWI) may be considered (*b*-values: 800-1000) for detection of local tumour invasion.

For PET-CT, non-attenuation-corrected images were identified as particularly useful for detecting chest wall invasion. Requests should specify whether talc pleurodesis has been performed. To mitigate post-treatment FDG avidity, imaging should be delayed 6-8 weeks post-surgery and 8-12 weeks post-radiotherapy.

The panel recommended saving images of any measurements obtained, as they are subject to higher inter-observer variation than most other tumour sites.[52]

## Future directions

### Photon counting CT

The advent of the photon-counting detector CT (PCD-CT) offers potential improvements and more accurate staging of mesothelioma by overcoming current imaging limitations. The dual-source PCD-CT (NAEOTOM Alpha, Siemens Healthineers, Forchheim, Germany) has inherent standard resolution of 144 detector rows and each with 0.4 mm slice

thickness, and capable of ultra-high resolution (UHR) scan of thinner collimation, which consisted of 120 detector rows with 0.2 mm slice thickness.[53,54] Thoracic imaging with high spatial resolution has shown improved depiction of anatomical structures, lung nodules and identification of fine traction bronchiectasis and reticulation in interstitial lung disease compared to the conventional energy integrating scintillation detectors (EIDs) CT scanner.[55,56] The image quality in terms of signal to noise ratio (SNR) could be further optimized with specific reconstructive kernels.[57] The high spatial resolution combined with better SNR would provide more accurate assessment of the maximum pleural thickness measurements compared to conventional EIDs scanners. In addition, PCD-CT directly converts incident X-ray photon into electrical impulse, which allows spectral separation of the photons proportional to their pulse amplitude into respective energy bins.[53,54] Spectral analysis at the ideal photon energy (kiloelectronvolt, keV) of specific energy bins could allow identification of structures of interest.[53,54,56] Recent phantom study has shown that spectral imaging is an useful tool in the differentiation of empyema and non-infected pleura.[58] The potential of PCD-CT with improved contrast resolution and spectral analysis could help to differentiate malignant pleural disease from adjacent tissue such as the chest wall, diaphragm, and pericardial invasion (Figure 9). No current published literature investigates the clinical impact of PCD-CT in mesothelioma imaging. Further research of PCD-CT with paired imaging correlation with MRI study and subsequent surgical specimen and pathological staging would yield interesting and confirmation data in the area of mesothelioma diagnosis and staging.

## PET-MRI

Murphy et al[59] assessed PET-MRI and PET-CT staging accuracy for PM using the TNM 7 staging system. PET-MRI was concordant with surgical staging in 6 of 9 cases, outperforming PET-CT, which matched in only 3 of 9 cases. PET-MRI also showed superior accuracy in T staging, aligning with pathological T stage in 7 of 9 for PET-CT. Both modalities were equivalent in N staging, with concordance in 7 of 9 cases. The study noted apparent mismatch between FDG uptake and diffusion restriction in areas of talc deposition, suggesting a potential method to differentiate talc from tumour-related FDG avidity. Advances in free-breathing ultrashort echo time MRI sequences significantly improve imaging quality and spatial resolution over traditional dual echo gradient imaging, improving the visibility of pulmonary and pleural nodules in PET-MRI.[60]

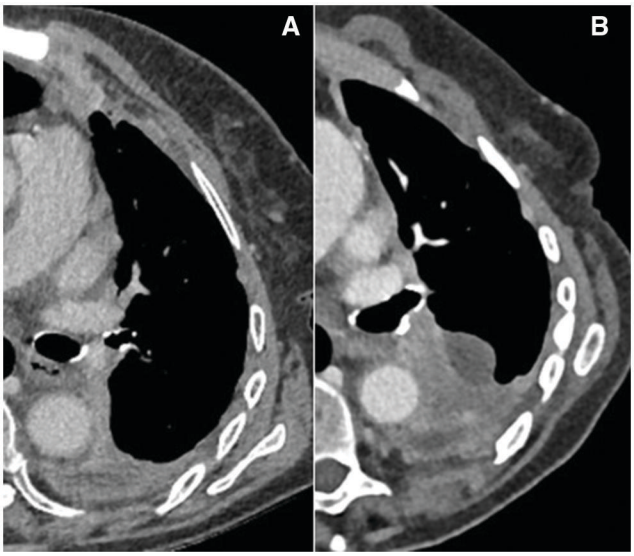


**Figure 9.** Energy integrating scintillation detectors (EIDs) CT (A) and photon-counting detector CT (PCD-CT) image (B). The left lateral pleural nodule is better appreciated on the PCD-CT image.

## Automated tumour segmentation

Prior to TNM 9, tumour size was not included in PM staging. Due to its rind-like circumferential growth pattern, tumour depth as a surrogate for volume, is less accurate,[61] especially in small-volume disease, where observer variability for lesion measurement can reach 20% at sites under 7 mm in thickness.[52] Additionally, pleural surface assessment is influenced by respiratory motion and patient positioning, which can lead to significant interobserver variability in measurement.[52,62,63] In addition, radiation-induced lung injury and pleural effusions can impair the accurate measurement of pleural tumour deposits. Studies have shown a correlation between tumour volume on CT and overall survival, emphasizing the importance of accurate measurements.[4,5,8,64] Semi-automated methods of volume measurement use manual contouring every few axial slices and interpolation to segment tumours, but these remain too time-consuming for routine clinical use.[24,65]

Deep convolutional neural networks (CNNs) are one method of classifying and segmenting lesions and other anatomy in medical images. Convolution focuses on small, local parts of an image, which helps to recognize patterns even if they change slightly, making them reliable and efficient for many image-related tasks. However, because they only look at small areas at a time, they struggle to understand relationships between distant parts of the image. CNN filters (which are "lookout" tools that scan images) use fixed settings or weights when analysing new images. These settings remain unchanged, irrespective of the specific image or situation. This rigid approach makes it harder for the network to adjust and accurately interpret the differences in medical images, where there can be a lot of variation due to different body types, diseases, or conditions. Transformers[66] were first used to help computers understand human language. Vision Transformers (ViTs)[67] use similar principles, adapted for image interpretation. Unlike CNNs, which can miss the big picture, ViTs break images into small patches and look at them as a sequence. This allows them to notice patterns and relationships across the whole image, not just in small parts. Both types of model have made substantial progress in various medical image tasks, including image classification, region of interest (ROI) detection and image segmentation.[68-71] The CNN-based U-Net model[72] is one of the most important early models. It utilizes an encoder (to learn the important features of an image) and a decoder (to reconstruct the identified important features back to the original image resolution). To keep small details clear, the model includes skip connections, which are shortcut links between matching layers in the 2 parts. Subsequent models have improved this approach using various techniques, such as residual connections (which help the model learn better),[73] 3D convolutional blocks,[74] and squeeze-and-excitation blocks (which helps the model focus on the most important features).[75] When using ViTs

instead of CNNs in this kind of model, they still follow the same overall U-shape. The difference is that parts of the model—the encoder, decoder, or both—are made using transformer blocks instead of the original CNN parts.

To help address the issue of data scarcity for training deep CNNs, researchers have investigated the use of convolutional layers pretrained on large natural image datasets, such as ImageNet[76-78] to initialize deep CNNs applied to clinical tasks through a process called "transfer learning."[79] This strategy can be used to directly extract feature descriptors of medical image regions-of-interest for further classification using a nondeep learning-based machine learning classifier (eg, in the classification of benign and malignant lesions) or to initialize the layers of a deep CNN that is subsequently fine-tuned for a given clinical task through further training.[80,81] These learned representations can then be transferred to the downstream task, resulting in improved performance and a deeper understanding of the medical data within its context.[82]

Previous methods of automated segmentation of PM on CT scans isolated pleural thickening by segmenting the lungs and the rib cage.[83] A deep CNN-based segmentation method based on U-Net architecture[84] has shown superior performance compared to the non-deep learning-based method on an independent test set of CT scans of PM patients with radiologist-provided tumour contours. However, there were higher levels of disagreement with observer-provided tumour contours in patients with pleural effusions.

Gudmundsson et al[85] have developed a CNN-based U-Net model to make tumour segmentation more accurate and automated in patients with an associated pleural effusion. The system was trained using 5230 individual CT scan slices from 126 patients with unilateral disease, with no evidence of invasion into chest wall or other structures (to reduce other potential confounders of automated segmentation). Image contrast was adjusted by rescaling Hounsfield unit values, making tumours more distinguishable. The system was then tested on 2 sets of patients, one with both tumour and pleural effusion and another general set for comparison. To measure performance, results were compared to manual tumour segmentation created by 3 expert radiologists. The accuracy was determined using the Dice Similarity Coefficient (DSC), a metric ranging from 0 (no overlap) to 1 (perfect overlap). The AI achieved a median DSC of 0.690, significantly improving upon a previous deep learning method.[84] Subsequent manual segmentation of tumour from fluid (by 5 radiologists on 69 axial CT sections) demonstrated a mean DSC of 0.712 when at least 1 radiologist manually excluded pleural effusion from tumour contours, and the mean DSC was 0.757 when none of the 5 observers excluded pleural effusion from tumour contour. This suggests fluid presence impacts tumour measurements, which is important when developing AI-based tools. Bland-Altman plots confirmed that the new AI method reduced bias and was less likely to overestimate or underestimate tumour size compared to earlier versions. The authors made no comment on CT technique in the methods, specifically the use of iv contrast and the timing of scan acquisition and these promising results need to be validated in a larger cohort.

The higher contrast resolution of MRI compared to CT is potentially better suited to volumetric analyses. Tsim et al[86] prospectively studied tumour volumes of 31 patients obtained from CT (portal venous phase only) and MRI (T1-weighted, isotropic, contrast-enhanced 3 T perfusion imaging) prior to any pleural intervention or treatment. Semi-automated MRI volumetry was performed, with manual contouring every 8-10 slices followed by linear interpolation on the intervening slices. Due to poor contrast resolution between tumour and adjacent structures on CT, manual segmentation was required,[87,88] taking a mean of 151 minutes per patient vs. 14 minutes for MRI. Mean MRI volumes were 23% larger than CT volumes and were independently associated with adverse survival, whereas CT volumes were not and were less reproducible. Blyth et al[89] have developed a fully automated imaging tool to assist in diagnosing PM using MRI perfusion analysis. The system evaluates 3 T, T1-weighted, fat-saturated, 3D spoiled gradient echo sequences before and after intravenous contrast, at multiple time points up to 13.5 minutes. Initially, a pleural effusion segmentation mask was created, with minimal user input to define a region of interest (ROI) for the pleura. This mask was extended to enclose the pleura, followed by subtraction of the original effusion volume. Using a dynamic spanning forest algorithm, supervoxels with similar signal intensity (SI) were generated, connected through time.[90] Mean signal intensity of supervoxels were classified as "ECE present" or "ECE absent," ECE being defined as peak SI at or before 4.5 min. At least one ECE-positive supervoxel classified the patient as malignant. This image-processing tool has the potential to facilitate clinical deployment of perfusion MRI as an early diagnostic tool for pleural mesothelioma.

## Conclusions

PM remains the most common primary tumour of the pleura and a cause of significant disease burden worldwide. There have been significant changes to the 9th edition of the TNM staging manual, requiring a worldwide change in practice when staging PM. This accelerates the need for effective, easy-to-use automated applications for tumour segmentation.

## Funding

None declared.

## Conflicts of interest

None declared.

## References

1. Health and Safety Executive. Mesothelioma statistics for Great Britain, 2024. https://www.hse.gov.uk/statistics/assets/docs/mesothelioma.pdf, accessed 1 March 2025.
2. International Association for the Study of Lung Cancer. In Asamura H, ed. *Staging Manual in Thoracic Oncology*. 3rd ed. Editorial Rx Press; 2024.
3. Rusch VW, Giroux D, Kennedy C, et al.; IASLC Staging Committee. Initial analysis of the international association for the study of lung cancer mesothelioma database. *J Thorac Oncol*. 2012;7:1631-1639. https://doi.org/10.1097/JTO.0b013e31826915f1
4. Gill RR, Naidich DP, Mitchell A, et al. North American multicenter volumetric CT study for clinical staging of malignant pleural mesothelioma: feasibility and logistics of setting up a quantitative imaging study. *J Thorac Oncol*. 2016;11:1335-1344. https://doi.org/10.1016/j.jtho.2016.04.027

5. Rusch VW, Gill R, Mitchell A, et al.; Malignant Mesothelioma Volumetric CT Study Group. A multicenter study of volumetric computed tomography for staging malignant pleural mesothelioma. *Ann Thorac Surg*. 2016;102:1059-1066.
6. Nowak AK, Chansky K, Rice DC, et al.; Staging and Prognostic Factors Committee, Advisory Boards and Participating Institutions. The IASLC mesothelioma staging project: proposals for revisions of the T descriptors in the forthcoming eighth edition of the TNM classification for pleural mesothelioma. *J Thorac Oncol*. 2016;11:2089-2099.
7. Gill RR, Yeap BY, Bueno R, et al. Quantitative clinical staging for patients with malignant pleural mesothelioma. *J Natl Cancer Inst*. 2018;110:258-264.
8. Pass HI, Temeck BK, Kranda K, et al. Preoperative tumor volume is associated with outcome in malignant pleural mesothelioma. *J Thorac Cardiovasc Surg*. 1998;115:310-317, discussion 317-318.
9. Francis RJ, Byrne MJ, van der Schaaf AA, et al. Early prediction of response to chemotherapy and survival in malignant pleural mesothelioma using a novel semiautomated 3-dimensional volume-based analysis of serial 18F-FDG PET scans. *J Nucl Med*. 2007;48:1449-1458.
10. Lee HY, Hyun SH, Lee KS, et al. Volume-based parameter of 18F-FDG PET/CT in malignant pleural mesothelioma: prediction of therapeutic response and prognostic implications. *Ann Surg Oncol*. 2010;17:2787-2794.
11. Murphy DJ, Gill RR. Volumetric assessment in malignant pleural mesothelioma. *Ann Transl Med*. 2017;5:241.
12. International Association for the Study of Lung Cancer. *IASLC Staging Manual in Thoracic Oncology*. 2nd ed. Rami-Porta R, ed. IASLC; 2016.
13. Armato S, Nowak K. Revised modified response evaluation criteria in solid tumours for assessment response in malignant pleural mesothelioma. *J Thorac Oncol*. 2018;13:1012-1021. https://doi.org/10.1016/j.jtho.2018.04.034
14. Gill RR, Nowak AK, Giroux DJ, et al. The international association for the study of lung cancer mesothelioma staging project: proposals for revisions of the 'T' descriptors in the forthcoming ninth edition of the TNM classification for pleural mesothelioma. *J Thorac Oncol*. 2024;19:1310-1325. https://doi.org/10.1016/j.jtho.2024.03.007
15. Sharma A, Fidias P, Hayman LA, et al. Patterns of lymphadenopathy in thoracic malignancies. *Radiographics*. 2004;24:419-434. https://doi.org/10.1148/rg.242035075
16. Billé A, Ripley RT, Giroux D, et al. Proposals for the 'N' descriptors in the forthcoming ninth edition of the TNM classification for pleural mesothelioma. *J Thorac Oncol*. 2024;19:1326-1338. https://doi.org/10.1016/j.jtho.2024.06.012
17. Kindler HL, Rosenthal A, Giroux DJ, et al.; Members of the IASLC Staging and Prognostic Factors Committee, Advisory Boards and Participating Institutions. The IASLC mesothelioma staging project: proposals for the M descriptors in the forthcoming ninth edition of the TNM classification for pleural mesothelioma. *J Thorac Oncol*. 2024;19:1564-1577.
18. Nowak AK, Giroux DJ, Eisele M, et al. The IASLC pleural mesothelioma staging project: proposal for revision of the TNM stage groupings in the forthcoming (ninth) edition of the TNM classification for pleural mesothelioma. *J Thorac Oncol*. 2024;19:1339-1351. https://doi.org/10.1016/j.jtho.2024.06.012.
19. Rintoul RC, Ritchie AJ, Edwards JG, et al.; MesoVATS Collaborators. Efficacy and cost of video-assisted thoracoscopic partial pleurectomy versus talc pleurodesis in patients with malignant pleural mesothelioma (MesoVATS): an open-label, randomised, controlled trial. *Lancet*. 2014;384:1118-1127.
20. Lim E, Waller D, Lau K, et al.; MARS 2 Investigators. Extended pleurectomy decortication and chemotherapy versus chemotherapy alone for pleural mesothelioma (MARS 2): a phase 3 randomised controlled trial. *Lancet Respir Med*. 2024;12:457-466.
21. Kindler HL, Ismaila N, Armato SG, et al. Treatment of malignant pleural mesothelioma: American society of clinical oncology clinical practice guideline. *J Clin Oncol*. 2018;36:1343-1373. https://doi.org/10.1200/JCO.2017.76.6394
22. Scherpereel A, Opitz I, Berghmans T, et al. ERS/ESTS/EACTS/ESTRO guidelines for the management of malignant pleural mesothelioma. *Eur Respir J*. 2020;55:1900953. https://doi.org/10.1183/13993003.00953-2019
23. Corson N, Sensakovic WF, Straus C, et al. Characterization of mesothelioma and tissues present in contrast-enhanced thoracic CT scans. *Med Phys*. 2011;38:942-947.
24. Labby ZE, Straus C, Caligiuri P, et al. Variability of tumor area measurements for response assessment in malignant pleural mesothelioma. *Med Phys*. 2013;40:081916. https://doi.org/10.1118/1.4810940
25. Tsim S, Stobo DB, Alexander L, et al. The diagnostic performance of routinely acquired and reported computed tomography imaging in patients presenting with suspected pleural malignancy. *Lung Cancer*. 2017;103:38-43.
26. Hallifax RJ, Talwar A, Rahman NM. The role of computed tomography in assessing pleural malignancy prior to thoracoscopy. *Curr Opin Pulm Med*. 2015;21:368-371.
27. Truong MT, Viswanathan C, Godoy MBC, et al. Pleural mesothelioma: role of CT, MRI, and PET/CT in staging evaluation and treatment considerations. *Semin Roentgenol*. 2013;48:323-334. https://doi.org/10.1053/j.ro.2013.03.017
28. Heelan RT, Rusch VW, Begg CB, et al. Staging of malignant pleural mesothelioma: comparison of CT and MR imaging. *AJR Am J Roentgenol*. 1999;172:1039-1047. https://doi.org/10.2214/ajr.172.4.10587144
29. Stewart D, Waller D, Edwards J, et al. Is there a role for preoperative contrast-enhanced magnetic resonance imaging for radical surgery in malignant pleural mesothelioma? *Eur J Cardiothorac Surg*. 2003;24:1019-1024. https://doi.org/10.1016/s1010-7940(03)00609-2
30. Coolen J, De Keyzer F, Nafteux P, et al. Malignant pleural mesothelioma: visual assessment by using pleural pointillism at diffusion-weighted MR imaging. *Radiology*. 2015;274:576-584. pp.https://doi.org/10.1148/radiol.14132111
31. Arenas-Jiménez JJ, García-Garrigós E, Escudero-Fresneda C, et al. Early and delayed phases of contrast-enhanced CT for evaluating patients with malignant pleural effusion: results of pairwise comparison by multiple observers. *BJR*. 2018;91:20180254. https://doi.org/10.1259/bjr.20180254
32. Husain AN, Colby TV, Ordóñez NG, et al. Guidelines for pathologic diagnosis of malignant mesothelioma: 2017 update of the consensus statement from the international mesothelioma interest group. *Arch Pathol Lab Med*. 2018;142:89-108.
33. Patel A, Roshkovan L, McNulty S, et al. Delayed-phase enhancement for evaluation of malignant pleural mesothelioma on computed tomography: a prospective cohort study. *Clin Lung Cancer*. 2021;22:210-217.e1. https://doi.org/10.1016/j.cllc.2020.06.002
34. Patel AM, Berger I, Wileyto EP, et al. The value of delayed phase enhanced imaging in malignant pleural mesothelioma. *J Thorac Dis*. 2017;9:2344-2349.
35. Armato SG, Blyth KG, Keating JJ 3rd, et al. Imaging in pleural mesothelioma: a review of the 13th international conference of the international mesothelioma interest group.. *Lung Cancer*. 2016;101:48-58.
36. Tsim S, Humphreys CA, Cowell GW, et al. Early contrast enhancement: a novel magnetic resonance imaging biomarker of pleural malignancy. *Lung Cancer*. 2018;118:48-56.
37. Wang ZJ, Reddy GP, Gotway MB, et al. Malignant pleural mesothelioma: Evaluation with CT, MR imaging, and PET. *Radiographics*. 2004;24:105-119. https://doi.org/10.1148/rg.241035058
38. Yamamuro M, Gerbaudo VH, Gill RR, et al. Morphologic and functional imaging of malignant pleural mesothelioma. *Eur J*

*Radiol*. 2007;64:356-366. https://doi.org/10.1016/j.ejrad.2007.08.010
39. Plathow C, Klopp M, Thieke C, et al. Therapy response in malignant pleural mesothelioma: Role of MRI using RECIST, modified RECIST, and volumetric approaches in comparison with CT. *Eur Radiol*. 2008;18:1635-1643.
40. Martin GA, Tsim S, Kidd AC, et al. Pre-EDIT: a randomized feasibility trial of elastance-directed intrapleural catheter or talc pleurodesis in malignant pleural effusion. *Chest*. 2019;156:1204-1213.
41. Gerbaudo VH, Katz SI, Nowak AK, et al. Multimodality imaging review of malignant pleural mesothelioma diagnosis and staging. *PET Clin*. 2011;6:275-297. https://doi.org/10.1016/j.cpet.2011.04.001
42. Erasmus JJ, Truong MT, Smythe WR, et al. Integrated computed tomography-positron emission tomography in patients with potentially resectable malignant pleural mesothelioma: staging implications. *J Thorac Cardiovasc Surg*. 2005;129:1364-1370.
43. Flores RM, Akhurst T, Gonen M, et al. Positron emission tomography defines metastatic disease but not locoregional disease in patients with malignant pleural mesothelioma. *J Thorac Cardiovasc Surg*. 2003;126:11-16. https://doi.org/10.1016/s0022-5223(03)00207-1
44. Ambrosini V, Rubello D, Nanni C, et al. Additional value of hybrid PET/CT fusion imaging vs. Conventional CT scan alone in the staging and management of patients with malignant pleural mesothelioma. *Nucl Med Rev Cent East Eur*. 2005;8:111-115.
45. Sørensen JB, Ravn J, Loft A, et al.; Nordic Mesothelioma Group. Preoperative staging of mesothelioma by 18F-fluoro-2-deoxy-D-glucose positron emission tomography/computed tomography fused imaging and mediastinoscopy compared to pathological findings after extrapleural pneumonectomy. *Eur J Cardiothorac Surg*. 2008;34:1090-1096. https://doi.org/10.1016/j.ejcts.2008.07.050
46. Lee ST, Ghanem M, Herbertson RA, et al. Prognostic value of 18F-FDG PETCT in patients with malignant pleural mesothelioma. *Mol Imaging Biol*. 2009;11:473-479.
47. The Royal College of Radiologists, Royal College of Physicians, British Nuclear, *Medicine* Society, Administration of Radioactive Substances Advisory Committee. Evidence Based Indications for the Use of PET-CT in the United Kingdom 2022. London: The Royal College of Radiologists; 2022.
48. Gerbaudo VH, Britz-Cunningham S, Sugarbaker DJ, et al. Metabolic significance of the pattern, intensity and kinetics of 18F-FDG uptake in malignant pleural mesothelioma. *Thorax*. 2003;58:1077-1082. https://doi.org/10.1136/thorax.58.12.1077.
49. Nowak AK, Francis RJ, Katz SI, et al. A multimodality imaging review of malignant pleural mesothelioma response assessment. *PET Clin*. 2011;6:299-311.
50. Wang Y, Carter BW, Muse V, et al. Potential pitfall in the assessment of lung cancer with FDG-PET/CT: Talc pleurodesis causes intrathoracic nodal FDG avidity. *Lung Cancer Int*. 2013;2013:683582.
51. Katz SI, Straus CM, Roshkovan L, et al. Considerations for imaging of malignant pleural mesothelioma: a consensus statement from the international mesothelioma interest group. *J Thorac Oncol*. 2023;18:278-298.
52. Armato SG, Nowak AK, Francis RJ 3rd, et al. Observer variability in mesothelioma tumor thickness measurements: defining minimally measurable lesions. *J Thorac Oncol*. 2014;9:1187-1194.
53. Leng S, Bruesewitz M, Tao S, et al. Photon-counting detector CT: system design and clinical applications of an emerging technology. *Radiographics*. 2019;39:729-743.
54. Willemink MJ, Persson M, Pourmorteza A, et al. Photon-counting CT: technical principles and clinical prospects. *Radiology*. 2018;289:293-312.
55. Mohammadzadeh S, Mohebbi A, Kiani I, et al. Direct comparison of photon counting-CT and conventional CT in image quality of lung nodules: a systematic review and meta-analysis. *Eur J Radiol*. 2025;183:111859.
56. Remy-Jardin M, Flohr T, Remy J, et al. Thoracic applications of Photon-Counting CT: Where are we after three years of clinical implementation? *Br J Radiol*. 2025;98:1813-1820.
57. Milos R-I, Röhrich S, Prayer F, et al. Ultrahigh-resolution photon-counting detector CT of the lungs: association of reconstruction kernel and slice thickness with image quality. *AJR Am J Roentgenol*. 2023;220:672-680.
58. Mihailovic JM, et al. Simultaneous high-pitch multi-energy CT pulmonary angiography using a dual-source photon-counting-detector CT: a phantom experiment. *J Appl Clin Med Phys*. 2024;25:e14496.
59. Murphy DJ, Mak SM, Mallia A, et al. Loco-regional staging of malignant pleural mesothelioma by integrated 18F-FDG PET/MRI. *Eur J Radiol*. 2019;115:46-52.
60. Burris NS, Johnson KM, Larson PEZ, et al. Detection of small pulmonary nodules with ultrashort echo time sequences in oncology patients by using a PET/MR system. *Radiology*. 2016;278:239-246. https://doi.org/10.1148/radiol.2015150489.
61. Abdel-Rahman O. Challenging a dogma: AJCC 8th staging system is not sufficient to predict outcomes of patients with malignant pleural mesothelioma. *Lung Cancer*. 2017;113:128-133.
62. Sensakovic WF, Starkey A, Roberts R, et al. The influence of initial outlines on manual segmentation. *Med Phys*. 2010;37:2153-2158.
63. Gill RR, Murphy DJ, Seethamraju RT, et al. Interobserver variability of quantitative and qualitative assessment using MRI in malignant pleural mesothelioma. *Radiol Cardiothorac Imaging*. 2020;2:e190066.
64. Liu F, Zhao B, Krug LM, et al. Assessment of therapy responses and prediction of survival in malignant pleural mesothelioma through computer-aided volumetric measurement on computed tomography scans. *J Thorac Oncol*. 2010;5:879-884.
65. Frauenfelder T, Tutic M, Weder W, et al. Volumetry: an alternative to assess therapy response for malignant pleural mesothelioma? *Eur Respir J*. 2011;38:162-168.
66. Vaswani A, Shazeer N, Parmat N, et al. Attention is all you need. *Adv Neural Inf Process Syst*. 2017;30:1–15.
67. Dosovitskiy A, Beyer L, Kolesnikov A, et al. 2020. An image is worth 16 × 16 words: transformers for image recognition at scale. arXiv, 2021, https://doi.org/10.48550/arXiv.2010.11929, preprint: not peer reviewed.
68. Shin H-C, Roth HR, Gao M, et al. Deep convolutional neural networks for computer-aided detection: CNN architectures, dataset characteristics and transfer learning. *IEEE Trans Med Imaging*. 2016;35:1285-1298.
69. Litjens G, Kooi T, Bejnordi BE, et al. A survey on deep learning in medical image analysis. *Med Image Anal*. 2017;42:60-88.
70. LeCun Y, Boser B, Denker JS, et al. Backpropagation applied to handwritten zip code recognition. *Neural Comput*. 1989;1:541-551.
71. Krizhevsky A, Sutskever I, Hinton GE. *Imagenet Classification with deep convolutional neural networks*. New York, NY, USA: Association for Computing Machinery, 2017. https://doi.org/10.1145/3065386
72. Ronneberger O, Fischer P, Brox T. U-Net: convolutional networks for biomedical image segmentation. In: *Medical Image Computing and Computer-Assisted Intervention—MICCAI 2015: 18th International Conference*, Munich, Germany, October 5-9, 2015. Proceedings, Part III, Vol. 18. Springer International Publishing, 2015:234-241.
73. He K, Zhang X, Ren S, et al. Deep Residual Learning for Image Recognition. In: *Proceedings of the IEEE Conference on Computer Vision and Pattern Recognition*, Las Vegas, 2016:770-778.
74. Çiçek Ö, Abdulkadir A, Lienkamp SS, et al. 3D U-Net: Learning Dense Volumetric Segmentation from Sparse Annotation. In: *Medical Image Computing and Computer-Assisted Intervention—MICCAI 2016: 19th International Conference*, Athens, Greece,

October 17-21, 2016. Proceedings, Part II, Vol. 19. Springer International Publishing, 2016:424-432.
75. Hu J, Shen L, Sun G. Squeeze-and-excitation networks. arXiv, 2019, https://doi.org/10.48550/arXiv.1709.01507, preprint: not peer reviewed2018:7132-7141.
76. Deng J, Dong W, Socher R, et al. ImageNet: a large-scale hierarchical image database. In: *Proceedings of the IEEE Conference on Computer Vision and Pattern Recognition, Miami, FL, USA*. 2009:248-255.
77. Ravishankar H, Sudhakar P, Venkataramani R, et al. 2017. Understanding the mechanisms of deep transfer learning for medical images. arXiv, arXiv:1704.06040, preprint: not peer reviewed.
78. Weiss K, Khoshgoftaar TM, Wang D. A survey of transfer learning. *J Big Data*. 2016;3:1-40.
79. Ravishankar H, Sudhakar P, Venkataramani R, et al. Understanding the mechanisms of deep transfer learning for medical images.. *LNCS*. 2016;10008:188-196. p
80. Antropova N, Huynh BQ, Giger ML. A deep feature fusion methodology for breast cancer diagnosis demonstrated on three imaging modality datasets. *Med Phys*. 2017;44:5162-5171.
81. Huynh BQ, Li H, Giger ML. Digital mammographic tumor classification using transfer learning from deep convolutional neural networks. *J Med Imaging (Bellingham)*. 2016;3:034501.
82. Chen L, Bentley P, Mori K, et al. Self-supervised learning for medical image analysis using image context restoration. *Med Image Anal*. 2019;58:101539.
83. Sensakovic WF, Armato SG, Straus C, et al. Computerized segmentation and measurement of malignant pleural mesothelioma. *Med Phys*. 2011;38:238-244.
84. Gudmundsson E, Straus CM, Armato SG, et al. Deep convolutional neural networks for the automated segmentation of malignant pleural mesothelioma on computed tomography scans. *J Med Imaging (Bellingham)*. 2018;5:034503.
85. Gudmundsson E, Straus CM, Li F, et al. Deep learning based segmentation of malignant pleural mesothelioma tumor on computed tomography scans: application to scans demonstrating pleural effusion. *J Med Imaging*. 2020;7:012705. https://doi.org/10.1117/1.JMI.7.1.012705
86. Tsim S, Cowell GW, Kidd A, et al. A comparison between MRI and CT in the assessment of primary tumour volume in mesothelioma. *Lung Cancer*. 2020;150:12-20.
87. Kidd AC, Tsim S, Blyth KG, et al. Technical limitation of semi-automated volumetric analysis using CT in patients with malignant pleural mesothelioma. Pleural Mediastinal Malignancy. *Eur Res J* 2019;54(suppl 63):PA3100. https://doi.org/10.1183/13993003.congress-2019.pa3100
88. Weber M-A, Bock M, Plathow C, et al. Asbestos-related pleural disease: value of dedicated magnetic resonance imaging techniques. *Invest Radiol*. 2004;39:554-564.
89. Armato SG, Katz SI, Frauenfelder T, et al. Imaging in pleural mesothelioma: a review of the 16th international conference of the international mesothelioma interest group. *Lung Cancer*. 2024;193:107832. https://doi.org/10.1016/j.lungcan.2024.107832
90. Belem FC, Guimaraes SJF, Falcao AX. Superpixel segmentation using dynamic and iterative spanning forest. In: *IEEE Signal Processing Letters*, Vol. 27, pp. 1440–4, 2020.


British Journal of Radiology, 2026, 99, 206–217
https://doi.org/10.1093/bjr/tqaf297
Review